DELPHI Collaboration

DELPHI 2003-055 CONF 675
DELPHI 2004-046 CONF 721
12 June, 2003

Single Intermediate Vector Boson Production in e^+e^- collision at $\sqrt{s}$ =183-209 GeV.

H.M. Blom, J. Timmermans [1]
NIKHEF, Postbus 41882, NL-1009 DB Amsterdam, The Netherlands
M. Bonesini
Dipartimento di Fisica G. Occhialini and INFN Sezione di Milano, I-20126 Milan, Italy
E. Migliore
Università di Torino and INFN Sezione di Torino, I-10125 Turin, Italy
A. Tonazzo
Università di Roma TRE and INFN Sezione di Roma 3, I-00146 Rome, Italy
M. Witek
Institute of Nuclear Physics, Krakow, Poland

Abstract

The production of single charged and neutral intermediate vector bosons in e^+e^- collisions has been studied in the data collected by the DELPHI experiment at LEP at centre-of-mass energies between 183 and 209 GeV, corresponding to an integrated luminosity of about 640 pb^{-1}. The measured cross-sections for the reactions, determined in limited kinematic regions, are in agreement with the Standard Model predictions.

Contributed Paper for ICHEP 2004 (Beijing).
Previously contributed to EPS 2003 (Aachen) and LP 2003 (FNAL)

---

[1]also CERN, CH-1211 Geneva 23, Switzerland

1 Introduction

Four-fermion processes became increasingly important in e^+e^- collisions at centre-of-mass energies above the Z pole. Even if they proceed through the full set of Feynman diagrams (Figure 1 [1]) particular topologies receive their dominant contribution from a subset of them. The production of a single vector boson[2] ($e^+e^- \to e^-\bar{\nu}_e W^+$, $e^+e^- \to e^+e^-\gamma^*/Z$) proceeds through the scattering of a quasi-real photon ($q_\gamma^2 \sim 0$) radiated from an incoming e^- on an e^+ of the other beam, i.e.: $\gamma e^+ \to \bar{\nu}_e W^+$, $\gamma e^+ \to e^+ Z$ [2]. The resulting topology is characterized by the e^- radiating the quasi-real photon predominantly lost along the beam line. The integrated luminosity delivered by the LEP collider in the run at centre-of-mass energies $\sqrt{s} \approx 200$ GeV (LEP2) allowed, for the first time, measurements of the cross-section of single boson production and not just the observation of distinctive events. The evaluation of the Standard Model cross-sections for these processes requires the computation of the full set of Feynman diagrams and, to deal with the collinear singularity, corresponding to the electron lost along the beam line, the usage of fully massive matrix elements. Besides, other two physical issues, the different scales of the couplings in the process and the scale for the QED initial state radiation, should be properly accounted for to provide a reliable prediction. Therefore the accurate prediction for single boson production was indicated as a benchmark for the codes used to describe four-fermion physics at LEP2 [3]. In addition single-W production provides access to the measurement of the trilinear gauge couplings at the $WW\gamma$ vertex; this measurement, in combination with other physics channels, has been made by the DELPHI Collaboration and is reported elsewhere [4]. Another motivation to study these processes is related to probing for new physics. Because of the large missing energy in the final state, the modelling of these processes is important to control the background in the search for the Higgs boson in the $H\nu\bar{\nu}$ channel and for physics beyond the Standard Model [5]. Finally single boson production is interesting as it will be the dominant source of weak bosons production at the forthcoming Linear Collider.

Single boson production is investigated in this paper in five different final states: $e^-\bar{\nu}_e q\bar{q}'$, $e^-\bar{\nu}_e l^+\nu_l$ ($l = \mu, \tau$) and $e^-\bar{\nu}_e e^+\nu_e$ for single-W production, $e^-e^+ q\bar{q}$ and $e^-e^+\mu^-\mu^+$ for single-Z production. Cross-sections are measured using the data collected by the DELPHI experiment at centre-of-mass energies ranging from 183 to 209 GeV with a corresponding integrated luminosity of about 640 pb^{-1}. The results update and supersede those already reported by the DELPHI Collaboration in [6].

The criteria for the selection of the events are mainly based on the information from the tracking system, the calorimeters and the muon chambers of the DELPHI detector. A detailed description of the DELPHI apparatus and its performances can be found in [7]. The detector has remained essentially unchanged in the LEP2 phase, except for upgrades of the Vertex Detector [8] and the addition of a set of scintillators counters to veto photons in the blind regions of the electromagnetic calorimetry at polar angles $\theta \simeq 40°$, $\theta \simeq 90°$ and $\theta \simeq 140°$. The main tracking device was the Time Projection Chamber (TPC). One of the sectors (1/12) of the TPC, hereafter indicated as S6, was not fully operational during the last period of data taking at $\sqrt{s} = 207$ GeV (about 50 pb^{-1}). These data were analysed separately, with the performance of the analysis being evaluated on dedicated simulation samples, where this effect was explicitly taken into account.

---

[2]Charge conjugate states are implied throughout the text.

2 Definition of the signal and simulation

Single boson production is investigated in this paper through four-fermion final states, $e^-\bar{\nu}_e f\bar{f}'$ and $e^+e^- f\bar{f}$. These final states receive contributions besides from single resonant diagrams from doubly resonant production, conversion diagrams and multiperipheral processes [1]. To enhance the single boson production contribution, and to enable consistent comparisons and combinations, it was agreed among the LEP collaborations to define the cross-sections in the limited kinematic regions described below.

$e\nu_e W$ channel: The four-fermion final states $e^-\bar{\nu}_e q\bar{q}'$ and $e^-\bar{\nu}_e l^+\nu_l$ $(l = \mu, \tau)$ can be produced both via single-W production, referred to as $e\nu_e W$ in the following, or via W-pair production. A distinctive feature of $e\nu_e W$ is the fact that the distribution of the electron direction is strongly peaked at small polar angles (θ_e) with respect to the incoming electron beam direction. Based on this consideration the $e\nu_e W$ signal was defined by the complete t-channel subset of the Feynman diagrams contributing to the $e^-\bar{\nu}_e q\bar{q}'$ and $e^-\bar{\nu}_e l^+\nu_l$ final states with additional kinematical cuts to exclude the regions of the phase space dominated by multiperipheral diagrams where the cross-section calculation is affected by large uncertainties:

$$\begin{aligned}
m_{q\bar{q}'} &> 45 \text{ GeV}/c^2 \quad &\text{for} \quad & e^-\bar{\nu}_e q\bar{q}', \\
E_{l^+} &> 20 \text{ GeV} \quad &\text{for} \quad & e^-\bar{\nu}_e l^+\nu_l \;\; (l^+ = \mu^+, \tau^+),
\end{aligned} \tag{1}$$

where $m_{q\bar{q}'}$ is the $q\bar{q}'$ invariant mass and E_{l^+} the lepton energy.
Single-W production accounts for more than 80% of all $e^-\bar{\nu}_e q\bar{q}'$ and $e^-\bar{\nu}_e l^+\nu_l$ events in the kinematic region defined above.

$e\nu e\nu$ channel: In the kinematic region with one electron lost in the forward direction, this final state receives, besides single-W production, a large contribution from Zee production (with $Z \to \nu_e\bar{\nu}_e$) and from the interference between single-W and Zee processes. Also in this channel the signal was defined by the complete t-channel subset of the Feynman diagrams with the additional kinematical cuts [3]:

$$|\cos\theta_{e^+}| < 0.95, \quad E_{e^+} > 20 \text{ GeV and } \; |\cos\theta_{e^-}| > 0.95 \; (\text{veto on } e^-). \tag{2}$$

Zee channel: The neutral bosons are produced in the so-called electroweak Compton scattering process $e\gamma \to e\gamma^*/Z$, where a quasi-real photon is radiated from one of the beam electrons and scattered off the other beam. The signature of such events is an electron in the detector, typically of low energy, recoiling against the γ^*/Z system, with the other electron usually lost in the beam-pipe. The Zee cross-section commonly agreed by the LEP experiments refers to the entire set of 48 graphs [4] contributing at tree level to the $e^+e^- f\bar{f}$ $(f = q, \mu)$ final state with the following restrictions in the phase space to enhance the single boson contribution:

$$\begin{aligned}
& m_{f\bar{f}} > 60 \text{ GeV}/c^2 \;\; \text{and} \tag{3} \\
\theta_{e^+} > 168°, \;\; & 60° < \theta_{e^-} < 168° \;\; and \; E_{e^-} > 3 \text{ GeV} \quad \text{for a visible electron, or} \\
\theta_{e^-} < 12°, \;\; & 12° < \theta_{e^+} < 120° \;\; and \; E_{e^+} > 3 \text{ GeV} \quad \text{for a visible positron.}
\end{aligned}$$

---

[3] Assuming a reference frame, as the one used in DELPHI, with the z axis oriented along the incoming e^- beam.

[4] Diagrams involving Higgs boson exchange are neglected.

the 12° (168°) being motivated by the lower angle of the acceptance for the electron identification of the LEP experiments.

At $\sqrt{s} = 200$ GeV, within this kinematic limits, the bremsstrahlung contribution amounts to about 97% for $e^+e^-q\bar{q}$ and 67% for $e^+e^-\mu^+\mu^-$ final states. The cut on the invariant mass was chosen at 60 GeV/c^2 both because it guarantees an efficient rejection of the multiperipheral contribution and because it provides a natural separation between the γ^*ee and Zee regions, as it corresponds to the minimum of the differential $m_{f\bar{f}}$ distribution. In this paper, for the $e^+e^-q\bar{q}$ final state, besides the above defined Zee cross-section, a measurement of the cross-section with the same acceptance cuts for e^+ and e^- but in the invariant mass range $15 < m_{q\bar{q}} < 60$ GeV/c^2 (hereafter referred to as γ^*ee) will be presented as well.

For both the $e\nu_eW$ and Zee samples, signal events were simulated with the WPHACT [9] event generator. For background processes, different generators were used: KK2f [10] for $q\bar{q}(\gamma)$, $e^+e^- \rightarrow \mu^+\mu^-(\gamma)$ and $\tau^+\tau^-(\gamma)$, TEEGG [11] and BHWIDE [12] for $e^+e^- \rightarrow e^+e^-\gamma$, PYTHIA 6.143 [13] and BDK [14] for two-photon collisions. Fragmentation and hadronization for the KK2f and WPHACT samples were performed using PYTHIA 6.156. A detailed description of the simulation of four-fermion events at LEP2 as done in DELPHI is given in [15]. All the events were processed through the full DELPHI detector simulation and analysis chain [7].

3 Single-W analysis

3.1 Selection of hadronic events

The experimental signature of $e\nu_eq\bar{q}'$ events consists of a pair of acoplanar jets. The undetected neutrino results in a large missing momentum at large angle to the beam direction.

Other physics processes which can give rise to a similar topology are $Z(\gamma)$ with $Z \rightarrow q\bar{q}$, WW events with at least one W decaying into hadrons, other four-fermion final states from neutral current processes [5] ($l^+l^-q\bar{q}$, $\nu\bar{\nu}q\bar{q}$, the latter being topologically identical to the signal) and events induced by two-photon collisions, hereafter called two-photon events. Some of these processes have cross-sections larger than that of the signal by several orders of magnitude. A selection based on an Feed-Forward Artificial Neural Network [17] was applied to reject them.

A sample of hadronic events was preselected by requiring at least seven charged particles to be measured in the detector. Events from Bhabha scattering were rejected by a cut on the total electromagnetic energy, $E_{EM}/\sqrt{s} < 50\%$. The contribution from two-photon collisions was reduced by requiring the total visible energy to be larger than 20% of $\sqrt{s}$ and the total transverse energy to be at least 15% of $\sqrt{s}$. In addition, it was required that the opening angle of the cone around the beam axis containing 15% of the visible energy has to be larger than 10°: two-photon events are concentrated in the forward regions and have low values of this variable. The background from $e^+e^- \rightarrow q\bar{q}(\gamma)$ was reduced by requiring the cosine of the polar angle of the missing momentum to satisfy the condition

---

[5] The definition of neutral current (NC) and charged current (CC) four-fermion processes of Ref. [16] are used throughout the text.

$\sqrt{s}$ (GeV)	$e\nu qq$ signal	other CC	NC	$q\bar{q}(\gamma)$	Total MC	Data
183	9.5	66.8	5.0	74.2	157.0 ± 0.7	167
189	32.5	195.6	25.7	204.5	462.8 ± 2.0	467
192	5.3	31.9	4.1	31.0	73.0 ± 0.3	72
196	17.5	92.8	16.7	79.5	208.5 ± 0.9	221
200	21.2	102.8	20.4	77.4	223.8 ± 1.0	263
202	10.2	49.4	10.2	39.4	110.1 ± 1.0	119
205	18.1	80.2	18.1	63.5	180.6 ± 0.8	193
207	37.5	160.3	36.3	131.4	368.6 ± 1.5	376

Table 1: Number of events expected from the contribution of different channels and observed in the data after preselection of $e\nu_e q\bar{q}'$ events at the different centre-of-mass energies. "Other CC" indicates charged current processes different form the signal, "NC" neutral current processes. The quoted errors on the total number of expected events ("Total MC") are the ones due to limited Monte Carlo statistics.

$|\cos\theta_{miss}| < 0.98$ and the acoplanarity angle between the two hadronic jets to be larger than $10°$. $Z(\gamma)$ events, with $Z \rightarrow q\bar{q}$, were further suppressed by vetoing events with electromagnetic clusters with energy larger than 45 GeV or, if the ISR photon escaped undetected in the dead region between the barrel and end-cap electromagnetic calorimeters ($\theta \sim 40°$), by vetoing events with signals in the hermeticity counters in a cone of $30°$ around the direction of the missing momentum. Cuts on the maximum total multiplicity (< 50) and on the visible mass (between 30 and 100 GeV/c^2) were applied against the residual contamination of multi-jet events from WW or NC processes. Finally, WW events with one W decaying to leptons were suppressed by requiring no identified electron or muon with energy larger than 10% or 7.5% of $\sqrt{s}$ respectively. Particles were identified as muons if there was at least one muon chamber hit associated to a track or if the size and longitudinal profile of the HCAL energy deposits associated to a track were consistent with a minimum ionizing particle. Electron identification was based on the reconstructed showers in the electromagnetic calorimeters associated to charged particle tracks.

The expected composition of the residual sample after the preselection stage is shown in Table 1, together with the number of selected events at each centre-of-mass energy. At this level of the selection, the fraction of signal events is about 6-10 % at all the energy points.

The final selection of $e\nu_e q\bar{q}'$ events was based on a Neural Network analysis. The input variables were chosen to provide a good separation from the main residual backgrounds after preselection. The first set of variables discriminated the signal from $q\bar{q}(\gamma)$ events:

- effective centre-of-mass energy after ISR, $\sqrt{s'}$, scaled to the nominal one [18];

- sum of the particle momenta projected on the thrust axis, $P_L^{tot}/\sqrt{s}$;

- cosine of the polar angle of the missing momentum $|\cos\theta_{miss}|$;

- total missing momentum normalized to the centre-of-mass energy $P_{miss}^{tot}/\sqrt{s}$;

- total transverse momentum with respect to the beam axis $P_t^{tot}/\sqrt{s}$;

$\sqrt{s}$ (GeV)	Eff. (%)	σ_{bgd} (pb)	$\mathcal{L}_{int}$ (pb^{-1})	N_{MC}	N_{data}	$\sigma_{e\nu_e q\bar{q}'}$ (pb)
183	36.3 ± 1.4	0.470 ± 0.010	51.6	31.9 ± 0.6	28	$0.199^{+0.300}_{-0.199}$
189	37.0 ± 1.5	0.472 ± 0.011	153.8	96.4 ± 2.3	110	$0.657^{+0.190}_{-0.178}$
192	36.7 ± 1.0	0.468 ± 0.011	24.5	15.3 ± 0.4	15	$0.392^{+0.469}_{-0.392}$
196	35.2 ± 0.6	0.470 ± 0.009	72.0	47.0 ± 0.9	49	$0.598^{+0.290}_{-0.263}$
200	36.1 ± 0.6	0.468 ± 0.007	81.8	54.5 ± 0.8	58	$0.669^{+0.269}_{-0.247}$
202	37.5 ± 1.0	0.469 ± 0.010	39.7	26.4 ± 0.6	30	$0.764^{+0.391}_{-0.346}$
205	38.3 ± 1.6	0.522 ± 0.009	66.2	49.7 ± 0.9	62	$1.080^{+0.323}_{-0.297}$
207	39.2 ± 1.5	0.526 ± 0.010	129.7	100.5 ± 1.0	114	$0.900^{+0.217}_{-0.203}$

Table 2: Performance of the $e\nu_e q\bar{q}'$ event selection and measured cross-sections at the centre-of-mass energies considered in the analysis. The quoted errors on efficiencies and backgrounds are the ones due to limited Monte Carlo statistics.

- event Thrust;

- $|90° - \theta_{thrust}|$, where θ_{thrust} is the polar angle of the thrust axis.

A second set of variables suppressed $qq\tau\nu_\tau$ events, where the τ lepton produces an isolated particle or a low multiplicity jet, and $qq\nu\nu$ events, where the kinematic properties of the visible system should be consistent with the decay of a Z:

- maximum transverse momentum of any particle with respect to the nearest jet P_{tJ}^{max}, when the particles are clustered using the LUCLUS [19] algorithm with the parameter $d_{min} = 6.5$;

- invariant mass of the detected particles in the event rescaled with the visible energy $M_{vis} \cdot \sqrt{s}/E_{vis}$;

- Lorentz boost factor of the event in the laboratory frame $\beta = P^{tot}/E_{vis}$.

Distributions of some of these variables, at $\sqrt{s} = 200$ GeV, are shown in Figure 2. The distribution of the Neural Network output variable is shown in Figure 3. The whole data sample is included in the plot. The cut on the output variable was set at 0.5, the value for which the product of efficiency and purity was found to be maximum.

The efficiency of the selection for the signal, the expected background, the luminosity and the number of selected events in the data at the various centre-of-mass energies are reported in Table 2, together with the evaluated cross-section for the hadronic channel alone. Efficiencies and backgrounds at $\sqrt{s} = 207$ GeV were found to be compatible in the two periods with the sector S6 of the TPC on or off, and results have been merged in the table. The purity of the final selected sample is about 25%. The main contamination is due to $WW \to \tau\nu_\tau q\bar{q}'$ events.

3.2 Selection of leptonic events

The experimental signature of the leptonic channel $e^+e^- \to e^-\bar{\nu}_e l^+\nu_l$ is the presence of a high energy lepton accompanied by a large missing momentum and no other significant

energy deposition in the detector. The analysis was optimised for final state leptons that are electrons or muons. In both channels, the contribution from $e\nu_e\tau\nu_\tau$ events was considered as part of the background.

The main backgrounds for the leptonic channel are the radiative production of two leptons $e^+e^- \to l^+l^-(\gamma)$, $e^+e^- \to W^+W^-$ events and two-photon collisions.

Events were selected if exactly one well measured charged particle was reconstructed. The quality of the track measurement was assessed as follows:

- relative error on the momentum, $\Delta p/p$, smaller than 100%;

- track length greater than 20 cm;

- polar angle θ between 10° and 170°;

- impact parameter in the transverse plane, $|IP_{R\phi}|$, smaller than 4 cm, and that along the beam direction, $|IP_z|$, smaller than 3 cm / $\sin\theta$.

Loose identification criteria were applied, requiring associated hits in the muon chambers or a significant energy deposition in the electromagnetic calorimeter. For electrons, the acceptance was restricted to the barrel region, $|\cos\theta| < 0.72$, and the best determination of the electron energy was estimated by combining the momentum measurement from the tracking devices and the calorimetric energy. Any other energy deposit in the detector not related to the lepton candidate was required not to exceed 2 GeV. In addition, the presence of tracks not fulfilling the quality criteria listed above was used to veto the event. The acceptance was restricted to the kinematic region of W decays by requiring the lepton momentum to lie below 45% of $\sqrt{s}$ and its transverse momentum to exceed 12% of $\sqrt{s}$.

A large residual contamination was still present, due to cosmic ray events in the muon channel and to Compton scattering in the electron channel. The former were suppressed by tightening the selections on the track impact parameters to $|IP_{R\phi}| < 0.2$ cm and $|IP_z| < 2$ cm for the muons. Compton scattering can mimic the $W^+ \to e^+\nu_e$ signal when the photon balancing the electron in the transverse plane is lost in the dead region between the barrel and forward electromagnetic calorimeters. Therefore events were rejected if a signal was found in the hermeticity counters at an azimuthal angle larger than 90° from the electron.

Figure 4 shows the momentum distribution of selected single muons in data and simulation, while the energy of selected electrons is shown in Figure 5. The performance of the analysis at the various centre-of-mass energy values and the results obtained are reported in Tables 3 and 4 respectively. For the electron channel a difference was found for efficiencies and backgrounds corresponding to the two periods at $\sqrt{s} = 207$ GeV with TPC sector S6 on or off, and in Table 4 the weighted averages of the two is shown. Compatible values were found instead for the muon channel.

3.3   Study of systematic uncertainties

The main source of systematic uncertainty in the present measurement is the knowledge of the background level in the selected samples. In particular, as can be seen from Table 1, in the hadronic channel selection there is an excess of data of about 5% with respect to the expectation. The sample at this stage of the analysis consists mainly of background events. This excess was taken into account by rescaling the input variables to the Neural

$\sqrt{s}$ (GeV)		Eff. on μ (%)	σ_{bkg} (fb)	$\mathcal{L}_{int}$ (pb^{-1})	N_{MC}	N_{data}	$\sigma_{e\nu\mu\nu}$ (fb)
$l = \mu$	183	44.8 ± 2.8	18.8 ± 1.6	51.6	2.3 ± 0.2	7	261^{+129}_{-100}
	189	47.2 ± 1.7	19.1 ± 1.2	153.8	7.7 ± 0.4	5	29^{+36}_{-29}
	192	48.4 ± 2.7	18.6 ± 1.6	24.5	1.3 ± 0.1	1	46^{+114}_{-46}
	196	49.0 ± 1.6	20.2 ± 1.3	72.0	4.1 ± 0.2	4	72^{+67}_{-48}
	200	45.2 ± 2.5	22.8 ± 1.4	81.8	4.9 ± 0.2	7	141^{+82}_{-64}
	202	45.3 ± 1.7	24.0 ± 2.0	39.7	2.4 ± 0.2	5	226^{+144}_{-107}
	205	45.4 ± 1.7	20.3 ± 1.7	66.2	4.4 ± 0.3	2	22^{+59}_{-22}
	207	46.3 ± 1.8	23.0 ± 1.6	129.7	8.4 ± 0.4	8	84^{+53}_{-42}

Table 3: Performance of the $e^- \bar{\nu}_e \mu^+ \nu_\mu$ event selection at the centre-of-mass energies considered in the analysis. The quoted errors on efficiencies and backgrounds are the ones due to limited Monte Carlo statistics.

$\sqrt{s}$ (GeV)		Eff. on e (%)	σ_{bkg} (fb)	$\mathcal{L}_{int}$ (pb^{-1})	N_{MC}	N_{data}	$\sigma_{e\nu e\nu}$ (fb)
$l = e$	183	37.2 ± 3.3	36.4 ± 2.5	51.6	2.7 ± 0.5	3	58^{+108}_{-58}
	189	35.6 ± 2.1	38.6 ± 2.5	153.8	8.1 ± 0.4	13	129^{+72}_{-60}
	192	35.6 ± 2.1	43.1 ± 2.5	24.5	1.4 ± 0.5	1	0^{+141}_{-0}
	196	35.5 ± 2.1	44.4 ± 2.5	72.0	4.2 ± 0.4	4	32^{+92}_{-32}
	200	32.3 ± 1.9	41.1 ± 2.5	81.8	4.7 ± 0.4	6	100^{+105}_{-80}
	202	31.0 ± 2.0	40.9 ± 2.5	39.7	2.3 ± 0.7	3	112^{+169}_{-112}
	205	29.6 ± 3.0	38.3 ± 2.6	66.2	3.5 ± 0.3	3	23^{+107}_{-23}
	207	29.0 ± 2.1	38.4 ± 2.9	129.7	6.8 ± 0.3	11	160^{+97}_{-80}

Table 4: Performance of the and $e\nu e\nu$ event selection at the centre-of-mass energies considered in the analysis. The quoted errors on efficiencies and backgrounds are the ones due to limited Monte Carlo statistics.

Network by the data - Monte Carlo ratio, reoptimising the Neural Network output and recomputing the cross-section at the different centre-of-mass energies. The average effect on the cross-section was found to be 20 fb and it was considered as a systematic error fully correlated between the energy points.

Possible inaccuracies in the modeling of background processes were evaluated by comparing different Monte Carlo generators. The only effect was found in the $q\bar{q}(\gamma)$ channel. Using the ARIADNE [20] event generator instead of PYTHIA, we found a background estimate of 474 ± 14 fb instead of 468 ± 7 fb in the final $e\nu_e q\bar{q}'$ sample selected at 200 GeV. The largest of the statistical errors of the ARIADNE and JETSET samples was taken as systematic error.

The total systematic error on the background cross-section, due to the effect listed above and to the limited simulation statistics, amounts approximately to $\pm 3\%$ in the hadronic channel and $\pm 6\%$ in the leptonic channels (see Tables 2, 3 and 4, for the term due to the limited Monte Carlo statistics).

From a comparison of dimuon events in data and simulation, the tracking efficiency,

Systematic effect	Error on $\sigma_{e\nu q\bar{q}'}$ (pb)	Error on $\sigma_{e\nu_e\mu\nu_\mu}$ (pb)	Error on $\sigma_{e\nu_e e\nu_e}$ (pb)
$\Delta\sigma_{bkg}$ ($e\nu_e q\bar{q}'$) from preselection	0.020	-	-
$\Delta\sigma_{bkg}$ ($e\nu_e q\bar{q}'$) $\pm3\%$	0.039	-	-
$\Delta\sigma_{bkg}$ ($e\nu_e\mu\nu_\mu$) $\pm6\%$	-	0.0030	-
$\Delta\sigma_{bkg}$ ($e\nu_e e\nu_e$) $\pm6\%$	-	-	0.0076
$\Delta\varepsilon$ ($e\nu_e q\bar{q}'$) due to MC stat.	0.011	-	-
$\Delta\varepsilon$ ($e\nu_e l\nu_l$) due to MC stat	-	0.007	0.006
$\Delta\varepsilon$ ($e\nu_e l\nu_l$) due to ε_{track}	-	0.0016	0.0016
$\Delta\varepsilon$ ($e\nu_e l\nu_l$) due to ε_e	-	-	0.006
Luminosity $\pm0.6\%$	0.012	0.001	0.001
Total	0.047	0.008	0.012

Table 5: Contributions to the systematic uncertainty on the $e\nu q\bar{q}'$, $e\nu\mu\nu$ and $e\nu e\nu$ cross-sections at $\sqrt{s} = 200$ GeV.

ε_{track}, of DELPHI was found to be 0.5% higher in the simulation. This quantity was assumed as systematic error. This has a negligible effect on the background, while it affects the selection efficiency of the signal for leptonic decays of the W.

The uncertainty on the efficiency of the electron identification was estimated by comparing a sample of Bhabha events in data and simulation. The discrepancy was at the level of 2%.

The luminosity is known with a total relative error of $\pm0.6\%$.

3.4   Total single-W cross-section

The total single-W cross-section is defined as:

$$\sigma_{e\nu_e f\bar{f}'} = \sigma_{e\nu_e q\bar{q}'} + 2 \times \sigma_{e\nu_e\mu\nu_\mu} + \sigma_{e\nu_e e\nu_e} \tag{4}$$

where the factor two accounts for the $e\nu\tau\nu_\tau$ channel, not measured in the present analysis, assuming $\mu - \tau$ universality. This assumption introduces a theoretical error at the level of $\sim 3\%$ on the $e\nu\tau\nu_\tau$ estimation.

The effects of the uncertainties listed in the previous section on the measurement of the $e\nu f\bar{f}'$ cross-section at $\sqrt{s}$=200 GeV are given in Table 5. The total systematic error, obtained from the sum in quadrature of the individual contributions, is at the level of $\pm5\%$. For the measurement at the other centre-of-mass energies, the same relative error was assumed.

The values of $\sigma_{e\nu_e f\bar{f}'}$ measured at the different centre-of-mass energies together with their statistical and systematic error are shown in Table 6.

4   Single-Z analysis

In the single γ^*/Z analysis, decays of the vector boson into hadronic and $\mu^+\mu^-$ final states were considered. Both final states are characterized by an electron scattered at large angle

$\sqrt{s}$ (GeV)	$\sigma_{e\nu_e f\bar{f}'}$ (pb)
183	$0.78^{+0.41}_{-0.29} \pm 0.04$
189	$0.84^{+0.22}_{-0.20} \pm 0.04$
192	$0.48^{+0.54}_{-0.40} \pm 0.02$
196	$0.77^{+0.33}_{-0.28} \pm 0.04$
200	$1.05^{+0.33}_{-0.29} \pm 0.05$
202	$1.33^{+0.51}_{-0.42} \pm 0.07$
205	$1.15^{+0.36}_{-0.30} \pm 0.06$
207	$1.23^{+0.26}_{-0.23} \pm 0.06$

Table 6: Total single-W cross-section, as defined in the text (eq. 4), as measured at the different centre-of-mass energies considered in the analysis. The first error is statistical, the second systematic.

with respect to the incoming direction. The other electron, lost in the beam pipe, results in a missing momentum pointing along the beam line direction.

4.1   Selection of hadronic events

The experimental signature of these events consists of a pair of jets produced in the hadronic decay of the γ^*/Z recoiling against an electron. To maximize the sensitivity of the analysis in the widest possible range of invariant masses of the γ^*/Z, the event selection was performed in three steps:

1. a loose preselection of events;

2. the identification of an isolated electron;

3. the final selection of signal events, optimized differently in two ranges of the invariant mass of the hadronic system, $m_{q\bar{q}}$, according to the most relevant background process in each region.

The preselection of events consisted of the following requirements:

- at least five charged particles in the event with at least one in the TPC with a measured transverse momentum larger than 2.5 GeV/c, in order to select hadronic events;

- the presence of at least one electron candidate selected by requiring energy depositions in the electromagnetic calorimeters $E_e > 3$ GeV, with an associated charged particle and in the angular acceptance $|\cos\theta_e| < 0.985$ defined by the acceptance of the DELPHI forward electromagnetic calorimeter;

- in order to reject events from Bhabha scattering, in events with more than one electromagnetic shower reconstructed, the energy of the second most energetic one was required to be less than $0.6E_{beam}$.

The electron candidates were then retained if they satisfy the following criteria:

	γ^*/Zee	WW	$Z(\gamma)$	$\gamma\gamma$	Others	Total MC	Data
1997 183 GeV							
Preselection	24.2	202.9	560.5	160.3	149.9	1097.8	1238
e ident.	18.2	75.5	23.0	21.7	58.1	196.5	195
Signal selection	11.4±0.2	0.4 ±0.1	2.4±0.3	0.8±0.8	1.3±0.1	16.3±0.9	23
1998 189 GeV							
Preselection	73.5	647.4	1487.6	434.1	426.6	3069.2	3470
e ident.	55.9	244.2	65.7	62.6	168.2	596.6	577
Signal selection	34.9±0.4	1.4 ±0.2	6.5±0.7	3.3±1.2	4.5±0.5	50.7±1.5	54
1999 192-202 GeV							
Preselection	113.1	985.1	1946.4	669.4	608.1	4322.0	5016
e ident.	85.4	382.9	87.0	70.5	237.3	863.1	915
Signal selection	54.8±0.5	2.7 ±0.2	9.4±0.6	2.6±0.7	6.0±0.3	75.6±1.0	78
2000 205-207 GeV							
Preselection	110.1	938.2	1620.6	654.2	562.2	3885.3	4034
e ident.	83.5	374.4	75.5	78.7	212.5	824.6	786
Signal selection	54.6±0.5	2.9±0.2	8.8±0.5	1.9±0.9	6.1±0.2	74.3±1.1	76

Table 7: Number of events expected from the contributions of different channels and observed in the data at different stages of the γ^*/Zee selection (hadronic channel) for the different years of data taking. The number of expected γ^*/Zee events has been computed using a simulation sample generated with WPHACT [9]. The column labelled "$\gamma\gamma$" refers to resolved two-photon events. The column labelled "Others" includes in order of decreasing importance other four-fermion processes, namely $eeqq$ outside signal definition and γ^*/Zee with fully leptonic final state and events from Bhabha scattering. Details on the selection are provided in Section 4.

- in the barrel ($42° < \theta < 138°$) the track parameters matched those of the shower measured by the electromagnetic calorimeter (HPC), with the additional requirement, for showers with an energy higher than 30 GeV, that the energy deposited in the hadronic calorimeter did not exceed 10% of that deposited in the electromagnetic one;

- in the forward ($10° < \theta < 32°$ and $148° < \theta < 170°$) the shower, obtained after reclustering of the energy depositions compatible with a single electromagnetic shower, matched exactly one VD-VFT track and no more than one ID-TPC track [7];

- their angle, α, with respect to the closest charged particle with momentum $p > 0.5$ GeV/c had to lie in the range $15° < \alpha < 170°$ where the upper limit rejects events from Bhabha scattering left in the sample at this stage of the selection;

- their angle with respect to the second closest charged particle, with $p > 0.5$ GeV/c, had to be greater than $40°$.

Electrons from conversions or from decays were further suppressed by requiring their impact parameters with respect to the primary interaction vertex to be $|IP_{R\phi}| < 0.35$ cm

mass range (GeV/c^2)	γ^*/Zee	WW	$Z(\gamma)$	$\gamma\gamma$	Others	Total MC	Data
$15 < m_{q\bar{q}} < 60$	49.2±0.5	0.2±0.1	3.6±0.4	4.2±1.2	9.4±0.4	66.7±1.5	80
$m_{q\bar{q}} > 60$	106.5±0.5	7.2 ±0.4	23.5±1.0	4.3±1.3	8.5±0.2	150.1±1.8	151

Table 8: Number of events expected from the contributions of different channels and observed in the data at the end of the γ^*/Zee selection (hadronic channel) for the overall LEP2 sample, in the two invariant mass ranges. The number of expected γ^*/Zee events has been computed using a simulation sample generated with WPHACT [9]. The column labelled "$\gamma\gamma$" refers to resolved two-photon events. The column labelled "Others" includes in order of decreasing importance other four-fermion processes, namely $eeqq$ outside signal definition and γ^*/Zee with fully leptonic final state and events from Bhabha scattering.

in the transverse plane and $|IP_z| < 1$ cm along the beam line.

The charged and neutral particles were then clustered into two jets with the Durham algorithm [21], excluding the tag electron and rejecting events for which $D_{3\to2}^{join} < 10^{-4}$. A constrained kinematic fit of the event, imposing energy and momentum conservation, was then performed assuming a topology of signal events with two jets, a visible electron and one lost along the beam line. The four-momentum of the invisible electron was chosen to be $(0, 0, Q_e E, E)$ with Q_e the charge of the tagged electron. Fits with a χ^2 probability smaller than 10^{-5} were rejected. The final selection of signal events was then performed using for the tagged electron and for the hadronic system the variables after the constrained fit. It was required that:

- $Q_e \cos\theta_{miss} > 0.95$ with θ_{miss} being the polar angle of the missing momentum computed before the kinematic fit;

- $Q_e \cos\theta_e > -0.5$ with θ_e being the polar angle of the tagged electron.

For $m_{q\bar{q}} < 60$ GeV/c^2, where the dominant background consisted of resolved $\gamma\gamma$ collisions, events with $Q_e \cos\theta_e > 0.9$ and $E_e > 0.75 E_{beam}$ were also rejected. The distributions of these variables after the electron identification cuts are shown in Figure 6 for the real and simulated data. The quantity of selected events in the data and the expected contributions from the different backgrounds after each selection step are shown in Table 7 for the different years of data-taking, while Table 8 shows the composition of the entire sample after the final selection in the two mass ranges. An excess of data of about 10% is observed at preselection level mostly due to imperfectly simulated events from Bhabha scattering. The efficiency of the selection on the signal, the expected background and the number of selected events in the data at the eight centre-of-mass energies are reported in Table 9, together with the evaluated cross-section.

The distribution of the invariant mass of the hadronic system after the kinematic fit is shown in Figure 7 for the overall LEP2 sample. The peak in the invariant mass distribution around the Z mass corresponds to events for which the contribution of the Zee process is dominant.

$\gamma^*/Z \to q\bar{q}$ ($15 < m_{q\bar{q}} < 60$ GeV/c^2)

$\sqrt{s}$ (GeV)	Eff. (%)	σ_{bgd} (pb)	$\mathcal{L}_{int}$ (pb^{-1})	N_{data}	σ (pb)
183	30.3±0.8	0.015±0.002	52.0	11	$0.65^{+0.23}_{-0.19} \pm 0.03$
189	30.7±0.8	0.030±0.006	153.5	16	$0.24^{+0.09}_{-0.08} \pm 0.02$
192	32.1±0.8	0.027±0.006	25.1	6	$0.66^{+0.35}_{-0.26} \pm 0.04$
196	29.9±0.8	0.021±0.004	75.9	14	$0.55^{+0.18}_{-0.15} \pm 0.03$
200	29.4±0.8	0.026±0.005	82.8	6	$0.16^{+0.12}_{-0.09} \pm 0.02$
202	29.0±0.8	0.026±0.005	40.3	2	$0.08^{+0.15}_{-0.08} \pm 0.02$
205	29.8±0.7	0.021±0.004	75.9	12	$0.46^{+0.17}_{-0.14} \pm 0.03$
207 TPC OK	28.3±0.9	0.019±0.004	84.1	4	$0.23^{+0.09}_{-0.08} \pm 0.03$
TPC S6-off	36.8±0.9	0.030±0.014	51.4	9	

$\gamma^*/Z \to q\bar{q}$ ($m_{q\bar{q}} > 60$ GeV/c^2)

$\sqrt{s}$ (GeV)	Eff. (%)	σ_{bgd} (pb)	$\mathcal{L}_{int}$ (pb^{-1})	N_{data}	σ (pb)
183	27.2±0.4	0.078±0.017	52.0	12	$0.56^{+0.27}_{-0.22} \pm 0.07$
189	27.8±0.4	0.068±0.007	153.5	38	$0.64^{+0.15}_{-0.14} \pm 0.04$
192	28.1±0.4	0.063±0.006	25.1	6	$0.63^{+0.40}_{-0.30} \pm 0.04$
196	28.8±0.3	0.060±0.006	75.9	19	$0.66^{+0.21}_{-0.18} \pm 0.04$
200	29.7±0.5	0.072±0.006	82.8	20	$0.57^{+0.20}_{-0.17} \pm 0.03$
202	30.5±0.4	0.066±0.006	40.3	5	$0.19^{+0.21}_{-0.16} \pm 0.03$
205	30.7±0.3	0.072±0.006	75.9	14	$0.37^{+0.17}_{-0.15} \pm 0.03$
207 TPC OK	31.0±0.3	0.068±0.006	84.1	22	$0.68^{+0.15}_{-0.14} \pm 0.03$
TPC S6-off	29.8±0.3	0.060±0.004	51.4	15	

$\gamma^*/Z \to \mu^+\mu^-$ ($m_{\mu^+\mu^-} > 60$ GeV/c^2)

$\sqrt{s}$ (GeV)	Eff. (%)	σ_{bgd} (fb)	$\mathcal{L}_{int}$ (fb^{-1})	N_{data}	σ (fb)
183	27.4 ± 1.1	0.6 ± 0.2	0.054	1	< 297 at 95 % C.L.
189	26.2 ± 1.0	1.1 ± 0.4	0.1581	5	< 249 at 95 % C.L.
192	26.3 ± 1.0	0.7 ± 0.2	0.0258	0	< 338 at 95 % C.L.
196	26.7 ± 1.0	1.3 ± 0.3	0.0769	2	< 295 at 95 % C.L.
200	27.2 ± 1.0	1.2 ± 0.3	0.0843	1	< 202 at 95 % C.L.
202	26.7 ± 1.0	0.9 ± 0.2	0.0411	0	< 262 at 95 % C.L.
205	26.4 ± 1.0	0.6 ± 0.2	0.0767	1	< 231 at 95 % C.L.
207 TPC OK	26.1±1.0	1.1±0.3	0.0874	1	< 201 at 95 % C.L.
TPC S6-off	27.5±1.0	0.8±0.2	0.0544	2	

Table 9: Performance of the γ^*/Zee event selection at the centre-of-mass energies considered in the analysis. The period with TPC sector 6 down is indicated as "207 TPC-S6 off". Cross-sections for $\gamma^*/Z \to \mu^+\mu^-$ are expressed in femtobarns due to smaller values.

12

4.2 Selection of leptonic events

The search was restricted to events with γ^*/Z going into a $\mu^+\mu^-$ pair with invariant mass of $\mu^+\mu^-$ above 60 GeV/c^2. The general features are exactly the same as for the hadronic channel with jets replaced by muons. Thus a three-track signature, of two high momentum muons and one e^+ or e^-, scattered at large angle, is expected in the detector. The signal selection criteria on angular distributions were similar to those used in the hadronic channel.

In the preselection the event was required to have exactly three tracks fulfilling the following criteria:

- fractional error on the momentum $\Delta p/p < 50\%$,

- impact parameter in the transverse plane $|IP_{R\phi}| < 0.5$ cm and along the beam direction $|IP_z| < 3$ cm;

- at least one associated hit in the Vertex Detector.

The sum of the charges of the three particles was required to be ± 1. Possible photon conversions were removed according to the procedure described in [7] and requiring in addition the minimum opening angle of any track pair to be larger than 5°.

Since the event topology is clean, the particle identification required at least two tracks to be identified as leptons (μ or e) and at least one of them to be a muon. For muon identification loose criteria were applied as in the case of single-W production (see Section 3.2). The flavour of the possible unidentified track was inferred from partial information taking into account the combination of the charges of the observed particles. In the case of $\mu^+x^-e^{\pm}$ or $x^+\mu^-e^{\pm}$, the unidentified track x was treated as μ. For $\mu^+\mu^-x^{\pm}$ the track x was taken as $e^{\pm}$. Since the efficiency of the identification of the electrons was significantly smaller than for the muons, a majority of events with $\mu^+\mu^-$ pair detected and an unidentified electron was accepted this way, thus reducing dramatically the sensitivity of event selection to electron identification (less than 5% drop of signal selection efficiency was observed after forcing electron track to be always unidentified). In this way the loss of efficiency due to electron identification was minimal. At the preselection stage, the momentum of the $e^{\pm}$ candidate had to be greater than 2 GeV/c, and the invariant mass of $\mu^+\mu^-$ greater than 20 GeV/c^2.

Due to the stringent cut on low multiplicity of the event, the data reduction factor was large. For all energy points, 88 events were preselected and 94.0 ± 0.6 events were expected. At this stage most of the events came from the neutral current four-fermion processes with $e^+e^-\mu^+\mu^-$ in the final state but outside the kinematical limits of the signal definition (see Table 10). The remaining contributions came mainly from the neutral current four-fermion processes ($e^+e^- \to l_1^+l_1^-l_2^+l_2^-$ excluding $e^+e^-\mu^+\mu^-$ case) from two-fermion processes ($e^+e^- \to \mu^+\mu^-(\gamma)$, $e^+e^- \to \tau^+\tau^-(\gamma)$) and a small fraction from $e^+e^- \to W^+W^-$.

A kinematic fit was performed before applying the final selection cuts to the data. The lost electron along the beam line and no missing momentum in the transverse plane were assumed. The invariant mass of $\mu^+\mu^-$ was recalculated if the probability of the fit was above 0.001. Otherwise the original uncorrected $\mu^+\mu^-$ invariant mass was kept. The electron momentum was required to be greater than 3 GeV/c and the $\mu^+\mu^-$ invariant mass greater than 60 GeV/c^2 in agreement with the the signal definition requirements.

	γ^*/Zee	$(e^+e^-\mu^+\mu^-)_{\mathrm{bgd}}$	Others	Total MC	Data
1997 183 GeV					
Preselection	0.87 ± 0.03	6.3 ± 0.1	0.6 ± 0.1	7.8 ± 0.1	4
Final Selection	0.60 ± 0.02	0.008 ± 0.003	0.02 ± 0.01	0.63 ± 0.03	1
1998 189 GeV					
Preselection	2.6 ± 0.1	19.2 ± 0.4	1.8 ± 0.2	23.6 ± 0.4	24
Final Selection	1.7 ± 0.1	0.03 ± 0.01	0.14 ± 0.06	1.91 ± 0.09	5
1999 192-202 GeV					
Preselection	3.8 ± 0.1	26.3 ± 0.3	2.4 ± 0.1	32.5 ± 0.3	21
Final Selection	2.7 ± 0.1	0.04 ± 0.01	0.21 ± 0.03	2.93 ± 0.06	3
2000 205-207 GeV					
Preselection	3.7 ± 0.1	23.8 ± 0.3	2.3 ± 0.1	29.8 ± 0.3	39
Final Selection	2.6 ± 0.1	0.04 ± 0.01	0.15 ± 0.03	2.79 ± 0.06	4

Table 10: Number of events expected from the contributions of different channels and observed in the data at different stages of the γ^*/Zee selection (leptonic channel) for the different years of data taking. The column "$(e^+e^-\mu^+\mu^-)_{\mathrm{bgd}}$" shows the numbers for the background events coming from all processes with $e^+e^-\mu^+\mu^-$ in the final state not fullfiling the signal definition criteria. All other background sources are collected inside the column "Others".

Finally the allowed angular ranges for the direction of the Z/γ^* momentum and missing momentum were defined by the following conditions, in which Q_e represents the charge of the observed electron:

- $Q_e \cos\theta_{\mu^+\mu^-} < -0.8$ with $\theta_{\mu^+\mu^-}$ being the polar angle of the $\mu^+\mu^-$ system;

- $Q_e \cos\theta_{miss} > 0.8$ with θ_{miss} being the polar angle of the missing momentum computed before the kinematic fit;

- $Q_e \cos\theta_e > -0.5$ with θ_e being the polar angle of the tagged electron.

After the final selection the background contribution is expected to be less than 10% of the total selected events. The remaining background from processes with $e^+e^-\mu^+\mu^-$ in the final state which was dominant at the preselection level was reduced to about 1%.

The efficiency of the selection of the signal, the expected background and the number of selected events in the data for all centre-of-mass energies are reported in Table 9. Due to low statistics of selected events only the upper limits of cross-sections at 95 % C.L. are given for each individual energy point. In total 13 events were selected and 8.3 ± 0.1 events were expected from data in the energy range from 183 GeV to 207 GeV. The $\mu^+\mu^-$ invariant mass distribution is shown in Figure 7.

The distributions of the energy and of the signed angle, $Q_e \cos\theta_e$, of the tag electron after the kinematic fit for hadronic and $\mu^+\mu^-$ events with $m_{f\bar{f}} > 60$ GeV/c^2, are shown in Figure 8 for the overall LEP2 sample. The observed spectra are in a fairly good agreement with the predictions from the simulation.

4.3 Systematic uncertainties

The measurement uncertainty is dominated by the limited real data statistics.

In the hadronic channel three sources of systematic errors were considered: the efficiency in the electron selection procedure, the modelling of the contribution from two-photon events, which represents the largest background component in the low invariant mass region, and the modelling of the fragmentation in the $q\bar{q}(\gamma)$ contribution, which represents the largest background component in the high invariant mass region.

The uncertainty on the efficiency of the electron identification was estimated by comparing the number of selected events in the data and in the simulation for a sample enriched in WW events with at least one of the two W's decaying, directly or in cascade, into a final state containing an electron. The same criteria for electron identification and isolation were adopted as in the Zee analysis but the signal selection criteria were changed to maximize the product efficiency $\times$ purity of the WW selection. The relative difference in the efficiency was found to be $\Delta\varepsilon_e/\varepsilon_e = (-2.2 \pm 3.6)\%$ where the error accounts both for the data and the simulation statistics. Conservatively, the error on the difference was used for the computation of the systematic error.

The uncertainty in modelling of two-photon events could arise from the bad modelling either of the direct or of the resolved photon contribution. As described in [15] in the region of single tag the direct component was simulated using the WPHACT generator while the resolved component using PYTHIA 6.143. To match the direct and resolved components in the region $m_{q\bar{q}} < 40$ GeV/c^2 the WPHACT generator was run with constituent quark masses. The direct component of single tag events with $m_{q\bar{q}} > 40$ GeV/c^2 was instead simulated with the WPHACT generator using current quark masses. To gauge the effect of the different quark masses for the single tag low mass direct component, a fully simulated sample with current quark masses only was used to evaluate the effect both on signal efficiency and on the background cross-section. The change in the quark mass does not affect the γ^*/Zee signal at any stage of the selection, while the background at the end of the selection is increased by about 5 fb in each invariant mass region. Concerning the resolved photon component, at $\sqrt{s} = 200$ GeV the cross-section of this background amounts to about 10 fb in the γ^*ee signal region and 17 fb in the Zee one. A different generator TWOGAM [22] predicts in these regions background cross-sections of 5 fb and 9 fb respectively. Because of the similar topologies, assuming the same efficiency as for the signal, the difference between the two predictions, which is stable in the range $\sqrt{s} = 183 - 207$ GeV, was taken as systematic error.

The uncertainty in modelling the fragmentation in $q\bar{q}(\gamma)$ events was evaluated using a simulation sample produced with the ARIADNE generator. The background cross-sections were found to be larger, but within the statistical error, leading to a decrease of the measured cross-sections of 3 ± 5 fb in the low invariant mass region and 7 ± 13 fb in the high invariant mass one. The largest of the statistical errors of the ARIADNE and JETSET samples, 3 fb in the γ^*ee signal region and 9 fb in the Zee one, was taken as systematic error.

These three systematics together with the error on the luminosity were taken fully correlated at the different centre-of-mass energies while the errors on the background cross-section and on the signal efficiency due to the limited simulation statistics were considered uncorrelated among the different energies.

The contributions of the sources of systematic uncertainty in the hadronic channel at

Systematic effect	Error on σ (pb)	
	$15 < m_{q\bar{q}} < 60$ GeV/c^2	$m_{q\bar{q}} > 60$ GeV/c^2
$\Delta\varepsilon_e$	0.009	0.022
$\Delta\sigma_{bkg}$ $(\gamma\gamma)$ direct	0.005	0.005
$\Delta\sigma_{bkg}$ $(\gamma\gamma)$ resolved	0.005	0.008
$\Delta\sigma_{bkg}$ $(q\bar{q}\gamma)$ fragmentation	0.003	0.009
$\Delta\varepsilon$ due to simulation stat	0.007	0.008
$\Delta\sigma_{bkg}$ due to simulation stat.	0.020	0.026
Luminosity $\pm 0.6\%$	0.001	0.004
Total	0.024	0.038

Table 11: Contributions to the systematic uncertainty on the γ^*/Zee cross-sections in the hadronic channel, in the two ranges of invariant mass of the hadronic system, at $\sqrt{s} = 189$ GeV.

Systematic effect	Error on σ (fb)
$\Delta\varepsilon$ due to simulation stat	1.8
$\Delta\sigma_{bkg}$ due to simulation stat.	1.4
Luminosity $\pm 0.6\%$	0.7
Total	2.4

Table 12: Contributions to the systematic uncertainty at $\sqrt{s} = 189$ GeV on the predicted γ^*/Zee cross-section in the leptonic channel. The systematic errors were conservatively considered to be the same for all centre-of-mass energies. The systematic due to the uncertainty on the electron identification efficiency was measured to be negligible.

189 GeV are summarized in Table 11. The total systematic uncertainty amounts to $\pm 10\%$ in the region $15 < m_{q\bar{q}} < 60$ GeV/c^2 and to $\pm 6\%$ for $m_{q\bar{q}} > 60$ GeV/c^2.

The contributions of the different sources of systematic errors in the leptonic channel are summarized in Table 12. The main source of systematic error is the limited simulation statistics, both for the signal and for the background. The uncertainty on the efficiency of the electron identification was measured to be negligible using relaxed identification criteria. The total systematic uncertainty amounts to about $\pm 5\%$ per energy point. Assuming no energy correlation of the systematic errors the overall systematic uncertainty on the energy averaged cross-section was estimated to be $\pm 2.5\%$, an order of magnitude smaller than the statistical uncertainty.

5 Combined single boson cross-sections

The measured values for single boson cross-sections are compared with the Standard Model predictions obtained with WPHACT [9] as a function of the centre-of-mass energy. This dependency is shown in Figures 9 and 10 for single-W and single-Z respectively.

The theoretical uncertainty on the predictions amounts to 5%. The overall compatibility with the Standard Model was checked by considering the ratio $R = \sigma_{exp}/\sigma_{SM}$ of the measured to the predicted cross-sections. At each energy point a Poissonian probability function was constructed based on the number of observed events, the number of expected background events and the signal extraction efficiency. A maximum likelihood fit to the global probability function, being the product over all probability functions for individual energies convoluted with a multidimensional Gaussian describing the correlated and uncorrelated systematic errors, was performed. The results were:

$$R(e\nu_e q\bar{q}') = 1.36 \pm 0.18 \text{ (stat.)} \pm 0.06 \text{ (syst.)},$$

$$R(e\nu_e \mu\nu_\mu) = 1.06^{+0.27}_{-0.25} \text{ (stat.)} \pm 0.03 \text{ (syst.)},$$

$$R(e\nu_e e\bar{\nu}_e) = 1.07^{+0.38}_{-0.35} \text{ (stat.)} \pm 0.09 \text{ (syst.)},$$

$$R(eeq\bar{q}) = 1.22^{+0.17}_{-0.16} \text{ (stat.)} \pm 0.06 \text{ (syst.)} \qquad 15 < m_{q\bar{q}} < 60 \text{ GeV}/c^2,$$

$$R(eeq\bar{q}) = 1.00^{+0.12}_{-0.11} \text{ (stat.)} \pm 0.05 \text{ (syst.)} \qquad m_{q\bar{q}} > 60 \text{ GeV}/c^2,$$

$$R(ee\mu^+\mu^-) = 1.59^{+0.51}_{-0.43} \text{ (stat.)} \pm 0.03 \text{ (syst.)} \qquad m_{\mu^+\mu^-} > 60 \text{ GeV}/c^2,$$

showing a good agreement with the Standard Model predictions.

References

[1] F. Boudjema et al., in *Physics at LEP2*, Vol.1, p. 228, G. Altarelli, T. Sjöstrand and F. Zwirner eds., CERN 96-01 (CERN, Geneva, 1996).

[2] G. Altarelli, G. Martinelli, B. Mele and R. Ruckl, Nucl. Phys. **B262** (1985) 204;
E. Gabrielli, Mod. Phys. Lett. **A1** (1986) 465;
K. Hagiwara et al., Nucl. Phys. **B365** (1991) 544.

[3] E. Accomando et al., *Four-fermion production in electron-positron collisions*, Reports of the working groups on precision calculations for LEP2 Physics, S. Jadach, G. Passarino, R. Pittau (eds.) CERN 2000-009 (2000), 1.

[4] DELPHI Collaboration, P. Abreu et al., Phys. Lett. **B502** (2001) 9.

[5] R. N. Mohapatra, G. Senjanovic, Phys. Rev. **D23** (1981), 165;
S. Godfrey, P. Kalyniak, N. Romanenko, Phys. Rev. **D65** (2002) 33009.

[6] DELPHI Collaboration, P. Abreu et al., Phys. Lett. **B515** (2001) 238.

[7] DELPHI Collaboration, P. Aarnio et al., Nucl. Instr. Meth. **A303** (1991) 253;
DELPHI Collaboration, P. Abreu et al., Nucl. Instr. Meth. **A378** (1996) 57.

[8] P. Chochula et al., Nucl. Instr. Meth. **A412** (1998) 304.

[9] E. Accomando, A. Ballestrero and E. Maina, Comp. Phys. Comm. **99** (1997) 270;
E. Accomando, A. Ballestrero and E. Maina, Comp. Phys. Comm. **150** (2003) 166.

[10] S. Jadach, B. F. L. Ward and Z. Was, Phys. Lett. **B 449** (1999) 97;
S. Jadach, B. F. L Ward and Z. Was, Comp. Phys. Comm. **130** (2000) 260.

[11] D. Karlen, Nucl. Phys. **B289** (1987) 23.

[12] S. Jadach, W. Placzeck and B.F.L Ward, Phys. Lett. **B390** (1997) 298.

[13] T. Sjöstrand, Comp. Phys. Comm. **82** (1994) 74;
T. Sjöstrand, P. Edén, C. Friberg, L. Lönnblad, G. Miu, S. Mrenna and E. Norrbin, Comp. Phys. Comm. **135** (2001) 238.

[14] F.A. Berends, P.H. Daverveldt and R. Kleiss, Comp. Phys. Comm. **40** (1986) 271, 285, 309.

[15] A. Ballestrero, R. Chierici, F. Cossutti and E. Migliore, Comp. Phys. Comm. **152** (2003) 175.

[16] D. Bardin et al., *Event Generators for WW Physics*, in Ref. [1], Vol.2 p. 3 [hep-ph/9709270].

[17] C. Peterson, T. Rognvaldsson, L. Lönnblad. Comp. Phys. Comm. **81** (1994) 185.

[18] P. Abreu et al., Nucl. Instr. Meth. **A427** (1999) 487.

[19] T. Sjöstrand, Comp. Phys. Comm. **28** (1993) 229.

[20] L. Lönnblad, Comp. Phys. Comm. **71** (1992) 15.

[21] S. Catani, *The k_T algorithm for jet production and fragmentation*, CERN-TH 6895/93 (1993).

[22] S. Nova, A. Olshevski and T. Todorov, CERN Yellow Report 2000-009.
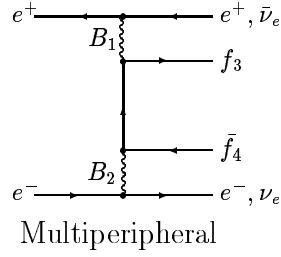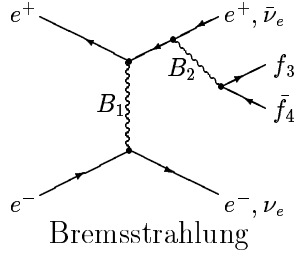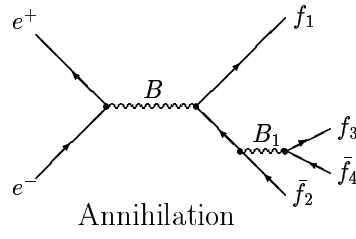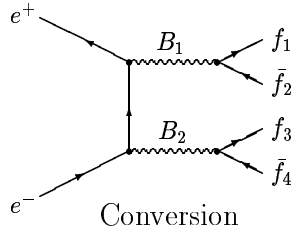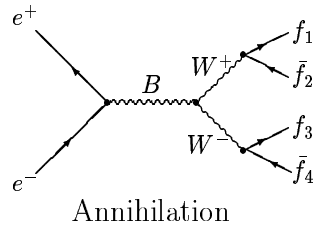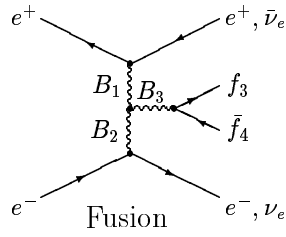
Figure 1: Four-fermion production classes of diagrams in e^+e^- annihiliation [1]: $B = Z, \gamma$ and $B_1, B_2, B_3 = Z, \gamma, W^\pm$. Diagrams involving Higgs boson exchange are not shown.
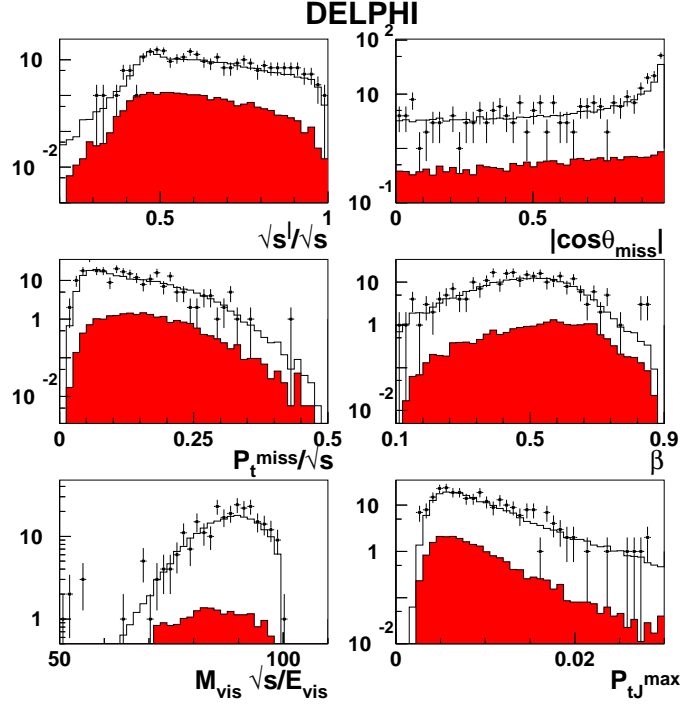
Figure 2: $e\nu_e W$ channel ($W \to q\bar{q}'$) at $\sqrt{s} = 200$ GeV. Distribution of some Neural Network input variables, as defined in the text, in real data (points with error bars) and in the simulation (histograms) after the preselection stage (see text). The distributions of these variables for the $e\nu_e W$ signal are shown as well (filled histograms).
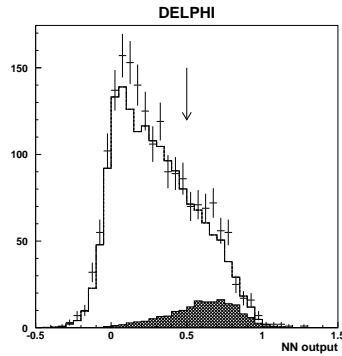
Figure 3: $e\nu_e W$ channel ($W \to q\bar{q}'$) in the overall LEP2 sample (about 620 pb^{-1} integrated luminosity). Distribution of the Neural Network output variable in real data (points with error bars) and in the simulation (histograms). The cross-hatched histogram represents the single-W signal, the open area is the background expectation. The arrow indicates the cut applied on this variable for the final event selection.
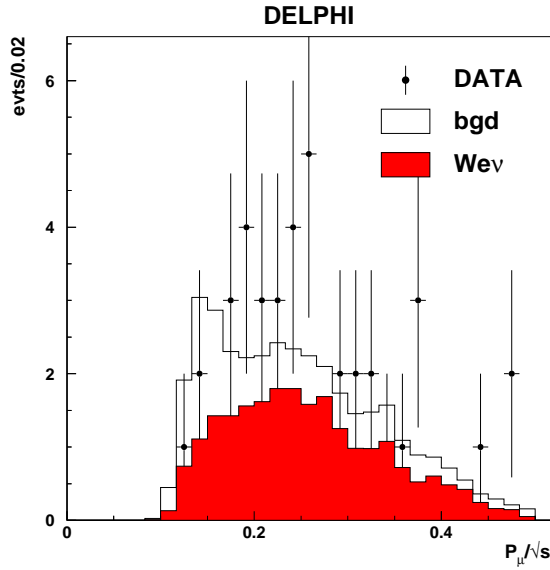
Figure 4: $e\nu_e W$ channel ($W \to l^+\nu_l$) in the overall LEP2 sample (about 620 pb^{-1} integrated luminosity). Momentum distributions of the lepton ($l^+ = \mu^+$) in real data (points with error bars) and in the simulation (histograms) for the events selected at the end of the analysis. The cross-hatched histogram represents the single-W signal, the open area is the background expectation.
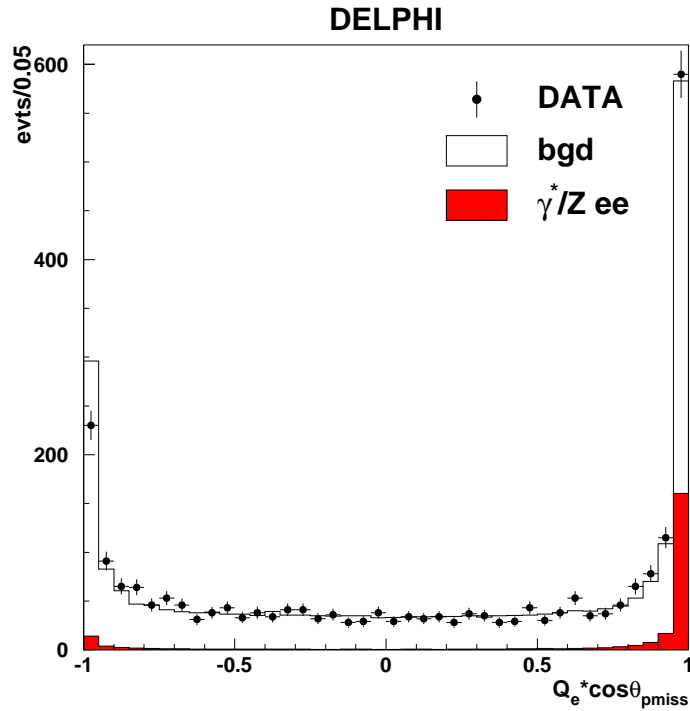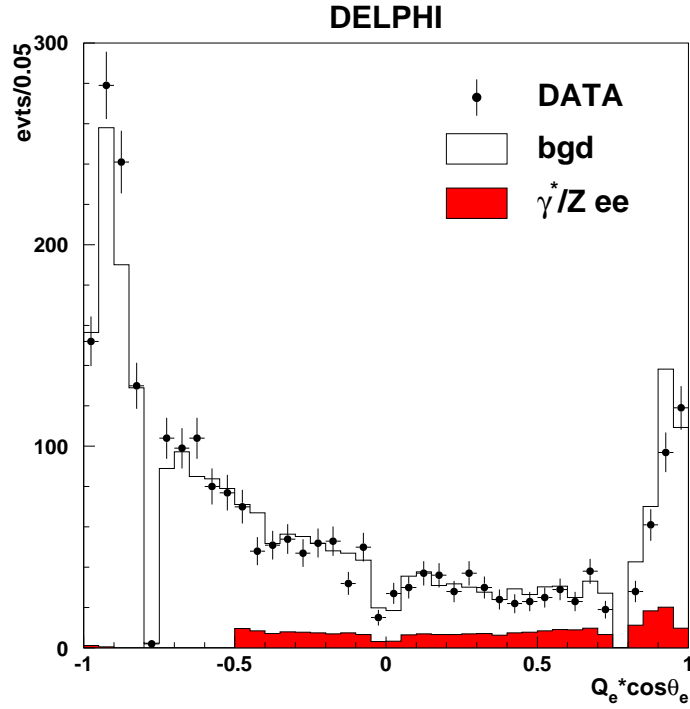
DELPHI PRELIMINARY
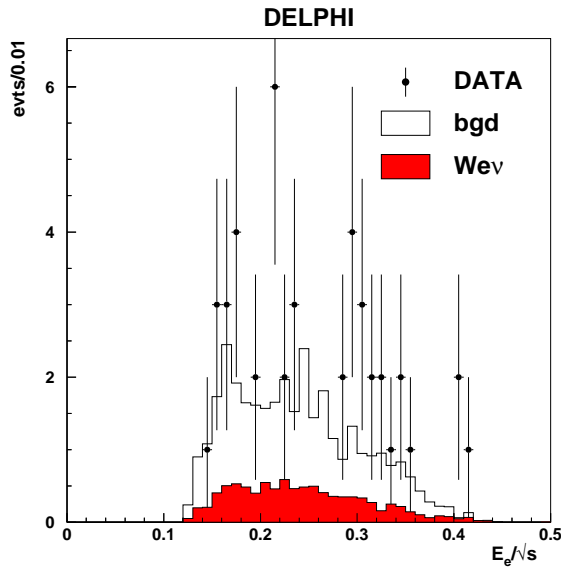
Figure 5: $e\nu_e W$ channel ($W \to l^+\nu_l$) in the overall LEP2 sample (about 620 pb^{-1} integrated luminosity). Energy distributions of the lepton ($l^+ = e^+$) in real data (points with error bars) and in the simulation (histograms) for the events selected at the end of the analysis. The cross-hatched histogram represents the single-W signal, the open area is the background expectation.

Figure 6: γ^*/Zee channel ($\gamma^*/Z \rightarrow q\bar{q}$) in the overall LEP2 sample (about 640 pb^{-1} integrated luminosity). Distributions of the variables used for the signal definition at the reconstruction level after the "electron identification" step (see Section 4.1), in real data (points with error bars) and in the simulation (histograms). The γ^*/Zee signal is defined in the kinematic region described in Section 2.
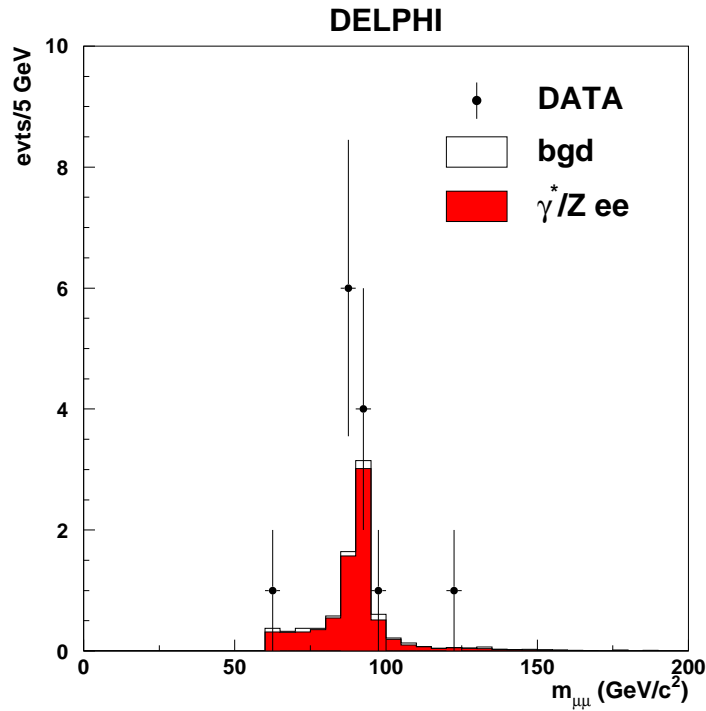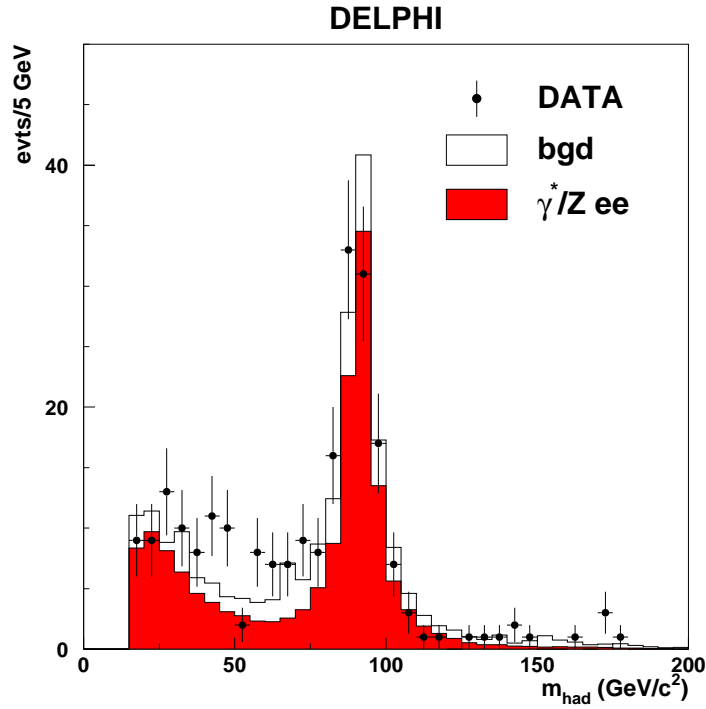
DELPHI PRELIMINARY

DELPHI

DELPHI

Figure 7: γ^*/Zee channel in the overall LEP2 sample (about 640 pb^{-1} integrated luminosity). Invariant mass distribution of γ^*/Z system in real data (points with error bars) and in the simulation (histograms) in the case of hadronic *(top)* and $\mu^+\mu^-$ *(bottom)* final states, in the selected signal sample.
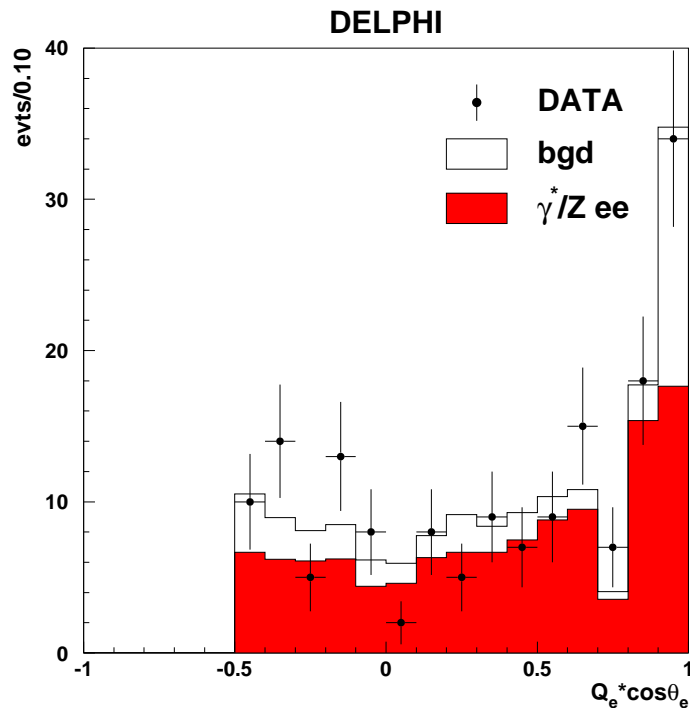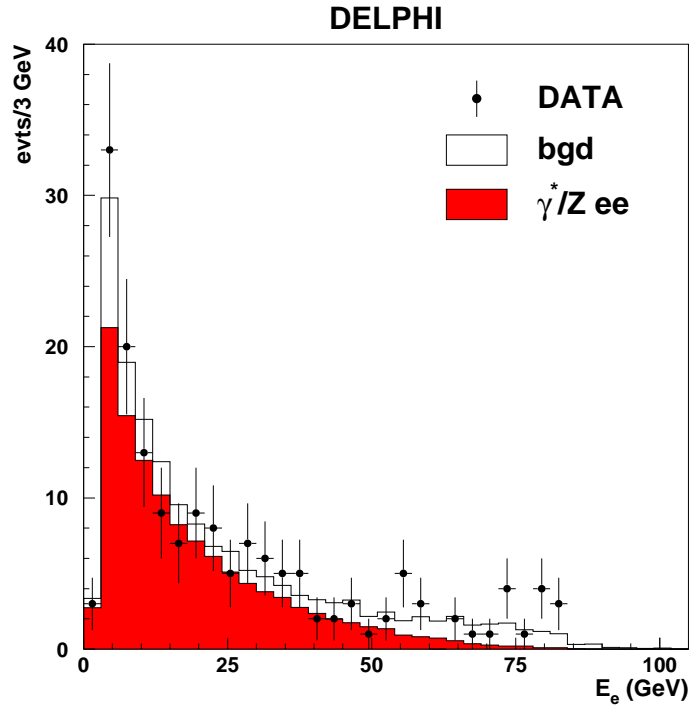
24

Figure 8: γ^*/Zee channel in the overall LEP2 sample (about 640 pb^{-1} integrated luminosity). Energy spectrum *(top)* and signed angle $Q_e \cos\theta_e$, *(bottom)* of the tag electron for hadronic and $\mu^+\mu^-$ final states with $m_{f\bar{f}} > 60$ GeV/c^2, in the selected signal sample. The points with error bars represent real data, the histograms the simulation.
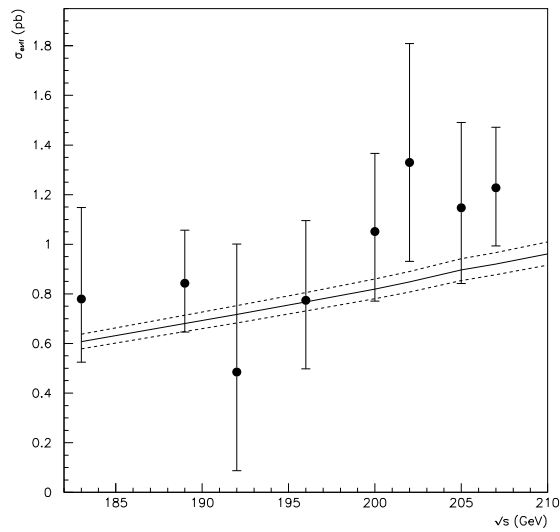
Figure 9: Cross-sections as a function of $\sqrt{s}$ for the $e\nu_e W$ channel. The solid curves are the Standard Model predictions computed with WPHACT [9].
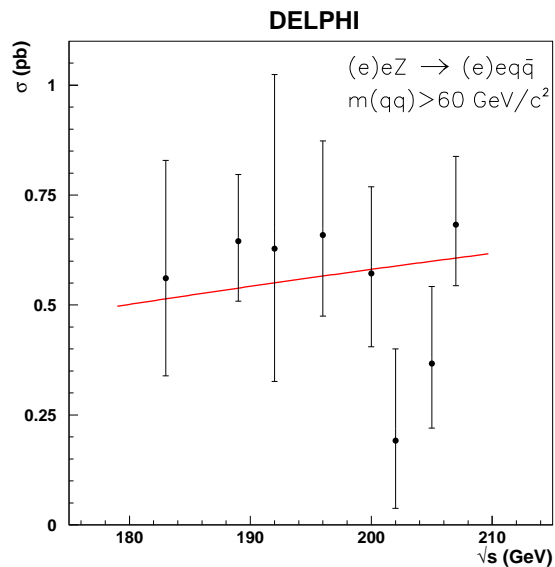
Figure 10: Cross-sections as a function of $\sqrt{s}$ for the Zee channel $Zee \rightarrow e^+ e^- q\bar{q}$. The solid curve is the Standard Model prediction computed with WPHACT [9].